Detection of graphene microelectromechanical system resonance

M. Wiesner,[1,2] N. Lindvall,[3] and A. Yurgens[3]
[1]*Faculty of Physics, Adam Mickiewicz University, Umultowska 85, PL61614 Poznań, Poland*
[2]*The NanoBioMedical Centre, Adam Mickiewicz University, Umultowska 85, PL61614 Poznań, Poland*
[3]*Department of Microtechnology and Nanoscience, Chalmers University of Technology, SE-412 96 Göteborg, Sweden*

We present an experimental setup for fast detection of resonances of graphene microelectromechanical structures of different quality. The relatively simple technique used to read-out of the resonance frequency is the main advantage of the proposed system. The resolution is good enough to detect vibrations of the graphene resonator with the quality factor of $\sim$24 and resonance frequency of 104 MHz.
© 2014 AIP Publishing LLC. [http://dx.doi.org/10.1063/1.4903987]

I. INTRODUCTION

Microelectromechanical systems (MEMS) are commercially used in sensor applications.[1,2] Recently, much research effort has been directed to their implementation in electronic devices, e.g., in wireless communication, medical devices,[3] and computer memory.[4] Electron-beam lithography and other advancements in fabrication technology have allowed reduction in the size of MEMS to nanoelectromechanical systems (NEMS). Since NEMS are just an order of 100 nm large, highly integrated sensor applications are possible. Moreover, low energy consumption of such devices is an advantage for continuous monitoring of important functions in hospitals,[5] aircrafts, or even human body.[6,7]

Owing to its exceptional mechanical[8] and electrical[9] properties, graphene is an excellent candidate to be used in MEMS, which are of great interest not only for fundamental studies of mechanics in the nanoscale but also for a variety of applications, e.g., mass sensing.[10] Graphene based MEMS have been the subject of interest[11–14] and their sensor applications have been reported in, e.g., Refs. 15 and 16. The most perspective are the gas sensor and airborne particle detection applications. There are two approaches to particles detection by graphene sensors. The first one is based on a change in the resistance of the sensor due to changes in graphene doping because of a charge transfer between particles or gas molecules and graphene.[17] The second one relies on changes in mechanical properties of suspended graphene membranes (MEMS resonators) as a result of additional mass of particles attached to the membrane.[10,18–20] The adsorption is reflected in changes in transfer characteristic of the equivalent field-effect transistor (FET).[15,21] The resonators are characterized by their eigenfrequency, amplitude of vibrations, and the quality factor.

To develop the gas sensors based on the vibrating graphene membranes, one has to take into account at least two issues.

The first is the resonance detection method. The most popular one is the mixing technique. Mixing in its simplest form is the multiplication of two harmonic signals entering a two terminal mixer device. Due the non-linearity of the I/V characteristics of the mixer, the converted output signal is proportional to the product of both input signals. This technique allows converting a high-frequency signal into a low-frequency one (the so-called down-mixing), which is much easier to detect. Mathematical background of this technique as well as its successful application to detection of the carbon nanotube resonance has been presented in Ref. 22. In the experiment, the carbon nanotube itself was used as the mixer. The measured signal consisted of several components, but only the one dependent on the displacement of the carbon nanotube was analysed.

There are many variants of the method. The common feature of experiments presented in the literature was the use of the investigated sample (carbon nanotube or graphene) as the mixing device. The experiments differed, however, in the instrument used to detect the resonance frequency. For example, Chen,[11] Sazonova,[23] and mentioned above Gouttenoire[22] used the lock-in and Xu[12] the vector network analyzer (VNA) to detect the resonance.

The radio frequency (RF) reflection readout method presented in Ref. 13 is another application of the mixing technique. However, in contrast to the above mentioned experiments, the double-clamped graphene was not a mixer, but the capacitive component of the tank circuit. The voltage applied to the tank circuit consisted of: a U_{DC} bias on the graphene capacitor, U_{AC} component actuating the graphene resonator at frequency f_m, and U_{LC} resulting from probing the tank RF signal at frequency f_{LC}. Vibrations of the graphene sheet led to the time varying gap between the back gate and graphene. The oscillation of the gap width gave rise to a time-varying capacitance. Consequently, the impedance of the LC circuit was modulated, which resulted in the side peaks in the reflected power observed at $f_{LC} \pm f_m$. Side bands were amplified, down-mixed, and then recorded by the RF lock-in amplifier.

The interferometric[14,24,25] method makes use of a laser light reflected from a vibrating graphene sheet. A laser at the drive frequency modulated the temperature of the graphene. Consequently, contraction/expansion of the sheet led to the graphene vibrations. Another laser beam was used for detection of motion. The light reflected from the vibrating graphene and from the substrate below the suspended graphene interfered, leading to a pattern sensitive to the position of

graphene. The motion of graphene was detected by changes in the intensity modulation of the reflected signal.

The second issue is the MEMS fabrication process. Production of a graphene MEMS with predefined characteristics is a difficult task as graphene quality depends on the fabrication process (i.e., chemical vapor deposition or mechanical exfoliation). The quality of graphene MEMS is measured by its resistance (R) dependence on the gate voltage (U_g) applied to the sample. A perfect sample shows a maximal resistance at $U_g = 0$ V, but often the maximum is shifted far away from $U_g = 0$ V because of the doping effect. Moreover, due to etching of SiO$_2$ beneath the graphene flake, the capacitance between the gate and graphene flake decreases leading to a week dependency of the resistance (R) on the U_g.

An application of a graphene-based MEMS as the gas sensor requires a portable device for detection of the resonance of the graphene MEMS. Mentioned above problems with fabrication of good quality graphene MEMS encouraged us to design and construct a portable experimental setup consisting of instruments affordable for most laboratories and capable of measuring the resonance of the graphene MEMS of different quality. The main component of the setup presented in this paper is the oscilloscope equipped with a fast Fourier transform (FFT) function. At the resonance, a large amplitude peak can be observed. A change in the resonance frequency due to, e.g., a mass absorption, can be directly observed on the oscilloscope screen.

The resolution of the setup is good enough to detect the resonance frequency of the graphene MEMS of the quality factor of ∼24 and resonance frequency 104 MHz.

II. SAMPLE PREPARATION

Graphene was produced by mechanical exfoliation on highly doped Si substrates with 290 nm dry thermal oxide. The single-layer graphene flakes were identified using the optical contrast of the flakes. In two subsequent e-beam lithography steps, graphene was patterned using a mild oxygen plasma followed by deposition of Au/Cr (or Au/Ti) electrodes (150/3 nm). The procedure allows obtaining a few of MEMS devices on one chip. Their resistance (R) vs. gate voltage (U_g) was measured revealing a clear maximum at the Dirac point ($U_g \approx 0$ V). To suspend a graphene sheet (Fig. 1), the substrate with graphene was placed in a buffered oxide etchant for 2 min. In this time, about 180 nm thick SiO$_2$ layer was removed from beneath the graphene sheet. The metal electrodes acted as a mask protecting SiO$_2$ lying below them. To stop further etching and to remove the etching residues, the sample was rinsed with DI water and then with ethanol. The chip prepared in this way was dried in a critical point dryer to minimize the risk of graphene damage due to stiction.

After the suspension, the $R(U_g)$ dependence does not show a usual maximum because of a strong parasitic p-doping effect resulting in a large shift of the Dirac point towards positive gate voltages. The device of the width $w = 0.5\,\mu m$ and length $L = 2\,\mu m$ showing the most pronounced $R(U_g)$ dependence $dR/dU_g = 107.5$ [Ω/V] was then selected for further investigation.
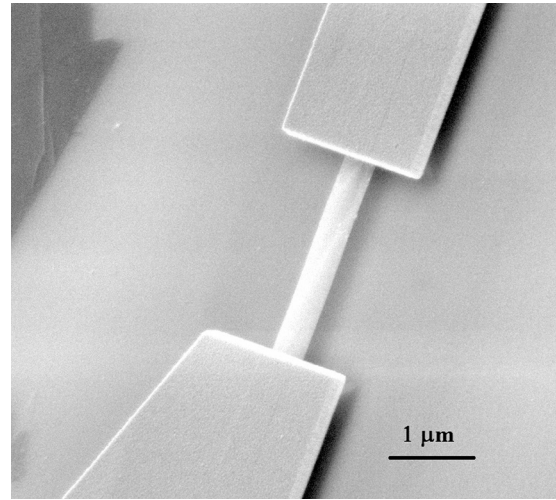

FIG. 1. The SEM image of a graphene micromechanical resonator. Metallic Ti/Au contacts clamped the graphene sheet 110 nm above the etched substrate.

The resonator dimensions determine its resonance frequency. According to the model presented in Ref. 12, the frequency scales as $1/L$ for thin vibrating graphene sheets of length ranging from 0.5 to 2 μm. Because for the graphene of 1.1 μm in length the resonance frequency was 65 MHz,[11] the expected resonance frequency of our device was of an order of 30–40 MHz. Of course, the graphene sheet in not the only vibrating component of the MEMS resonator. During the process of etching of the substrate, beneath the graphene sheet, a part of golden contacts clamping the graphene sheet becomes suspended. This part of the clamps vibrates with the frequency, which scales as t/L_{Au}^2 (where t and L_{Au} are the thickness and length of the suspended part of the golden clamp, respectively). To distinguish the graphene vibration from the clamp vibration, one has to analyze the gate dependence of the resonance frequency. For the golden contact, because of its large thickness, the tunability of the resonance by the gate voltage is much lower when comparing to the one-atom thick graphene sheet. Moreover, if the graphene sheet is narrow, vibrations of the clamp and graphene are well separated in the frequency domain, so one can observe only the graphene resonance.

III. EXPERIMENT

All measurements presented below were performed at room temperature and in vacuum of 3×10^{-4} mbar. To verify the elastic properties of fabricated MEMS and confirm the existence of its resonance, we use the setup described in Ref. 12 (see Fig. 2).

The bias current I_{bias} was applied to the source. Applied to the gate RF driving power P_{in} enforced vibrations of the graphene sheet. The voltage U_g was applied to the gate electrode to adjust both the tension and the conductance in the graphene sheet. The DC component of the output current was terminated by the resistor, whereas the AC component was amplified and recorded by the VNA. The amplified output current I_{tot} consisted of four components
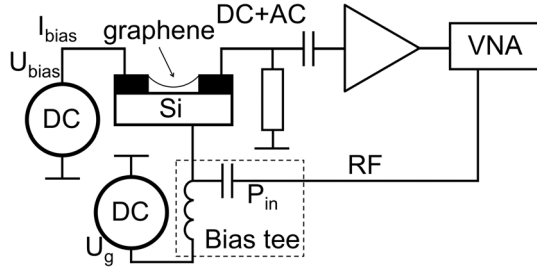
FIG. 2. Scheme of the experimental setup used for verification of elastic properties of fabricated MEMS.

$$I_{tot} = I_{Cb} + I_{mCg} + I_{graphG} + I_{mG}, \qquad (1)$$

where I_{Cb}—resulted from the capacitive background signal related to the capacitance between the gate and the drain (C_b), I_{mCg}—the current is induced by modulation of the gate capacitance caused by mechanical oscillations of the graphene, I_{graphG}—resulted from change of the graphene conductance (G) caused by change in the gate voltage, I_{mG}—resulted from the conductance (G) modulation caused by the gate capacitance oscillation due to graphene vibrations.

According to the model presented in Ref. 12, the third and fourth terms in Eq. (1) comprise the bias voltage. Because at the resonance only the fourth term (related to the graphene vibrations) varies as $U_{bias}U_g^2 dG/dU_g$, the direction of I_{bias} determines the shape of the magnitude (peak or dip) in the transmission measurements. The bias dependent shape of the magnitude observed in our measurements confirmed the resonance of the graphene sheet—Figs. 3(a) and 3(b).

The resonance frequency of the graphene resonator can be tuned by the gate voltage.[12] Because of a small value of dR/dU_g of our device the resonance frequency f_{r1} and the quality factor Q_1 shift are only weakly dependent on the gate voltage—Fig. 4.

The discrepancy between the expected (about 30–40 MHz) and measured resonance frequencies came from the tension T built in the graphene resonator. Two sources of the tension were identified: fabrication process and electric field applied to the gate. To extract its value, we used the beam approximation of MEMS,[26]
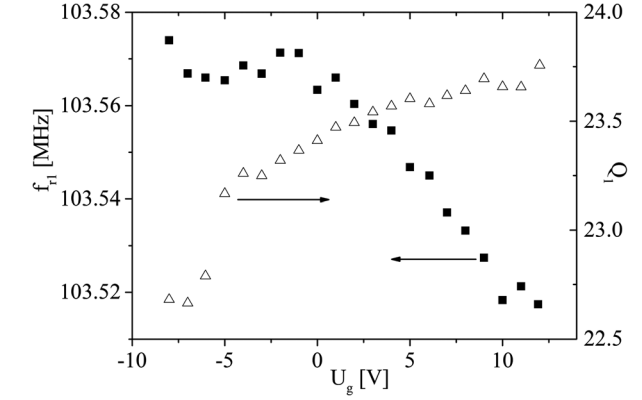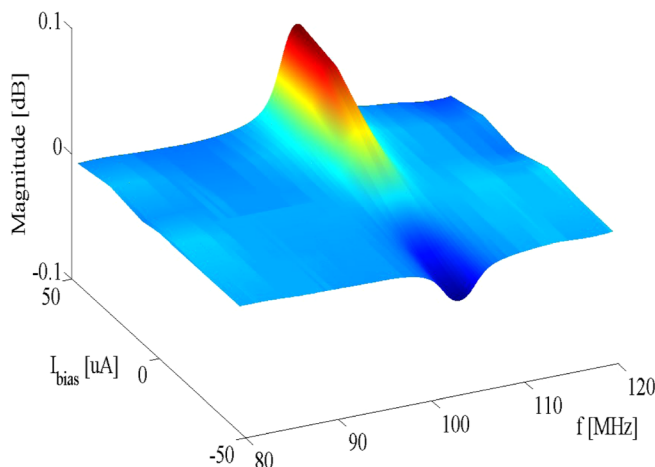

FIG. 4. The resonance frequency f_{r1} (full squares) and quality factor Q_1 (empty triangles) dependence on the gate voltage measured with the setup presented in Fig. 2.

$$f_{r1} \approx \left(1.03 \frac{t}{L^3} \sqrt{\frac{E}{\rho}} \right) \sqrt{1 + \frac{TL^2}{3.4 Et^3 w}}, \qquad (2)$$

where E and ρ are elastic (Young's) modulus and mass density of graphene, t, w, and L are the device thickness, width, and length, respectively. The extracted tension value was 40 nN, which was comparable to that reported in Ref. 27.

Having well characterized the microelectromechanical device, a new experimental setup was designed and constructed. The expensive VNA was replaced with an oscilloscope with a built-in FFT module (see Fig. 5). The suspended graphene was actuated by the potential difference between the sheet and the gate. The DC voltage U_g was applied to the gate electrode to adjust both the tension and the conductance in the graphene sheet. The input signal from the generator (AC) was split (PS) into two parts of the same amplitude A and frequency f_1:$v_1 = A \sin(2f_1 t)$. One part (the driving force) sets the graphene into motion at frequency f_1 and the second part was delivered to the first input of the mixer (M). The signal reflected from the device $v_2 = B \sin(2f_2 t)$ was decoupled with the directional coupler (C), amplified and delivered to the second input of the mixer (M). The output signal of the mixer has a form
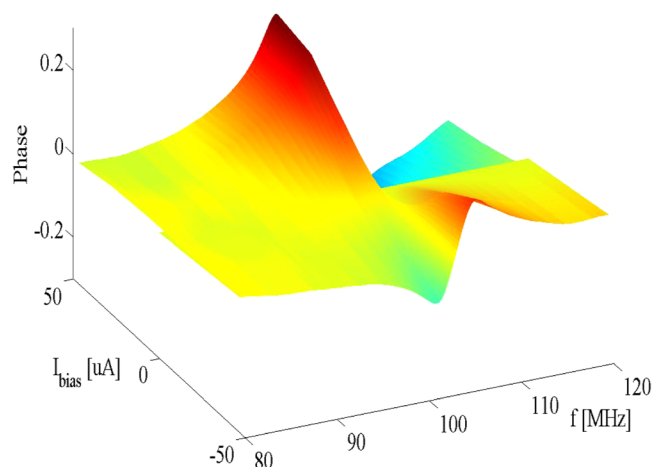

FIG. 3. Confirmation of the graphene MEMS resonance. The bias dependent shape of the magnitude (a) and phase (b) of the transmission parameter S_{21} observed using the first setup (Fig. 2). AC power applied to the gate $P_{in} = -15$ dBm, $I_{bias} = \pm 45\ \mu A$, and DC gate voltage $U_g = +12$ V.
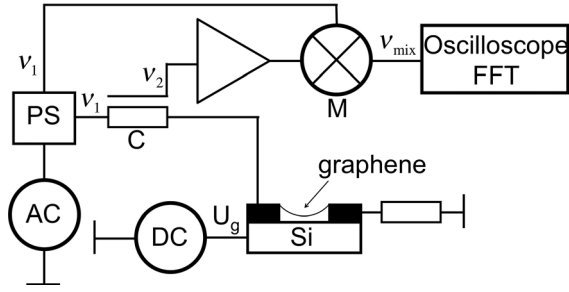
FIG. 5. Scheme of the new experimental setup. The amplitude of the mixed signal, observed on the oscilloscope equipped with FFT, reached a maximal value only at the resonance.

$$v_{mix} = \frac{1}{2}AB\{\cos[2\pi(f_1 - f_2)t] - \cos[2\pi(f_1 + f_2)t]\}. \quad (3)$$

The resonance frequency of the graphene resonator was determined by the gate voltage. The amplitude of the decoupled signal was low and its frequency different from f_1. Only at the resonance when $f_1 = f_2 = f_{r2} \approx 114$ MHz, the amplitude B reached a maximal value. The second component of the mixed signal (3) was observed in the fast Fourier transform spectra as a peak at the frequency $f_{mix} = f_1 + f_2 = 2f_{r2} = 228$ MHz (see Fig. 6).

The effect of the gate voltage on the resonance frequency is presented in Fig. 7.

IV. DISCUSSION

The difference between resonance frequencies measured in both experiments (Figs. 4 and 7) could be explained by slightly different conditions at which these experiments were performed.

First factor which should be taken into account when comparing results of both experiments is the time delay between the two experiments. The second experiment (Fig. 7) was performed 7 days after the first one (Fig. 4). In the meantime, the graphene resonator was exposed to ambient conditions. According to Ref. 11, if the gate voltage is large enough to induce tension in the graphene sheet, the resonance frequency shifts downwards. If U_g is not the dominant factor inducing the tension, mass adsorption results in the frequency shift towards larger values. As it was mentioned in Sec. II, the Dirac point of our resonator was shifted from $U_g = 0$ V toward positive values of the gate voltages. Weak dependence of the graphene resistance
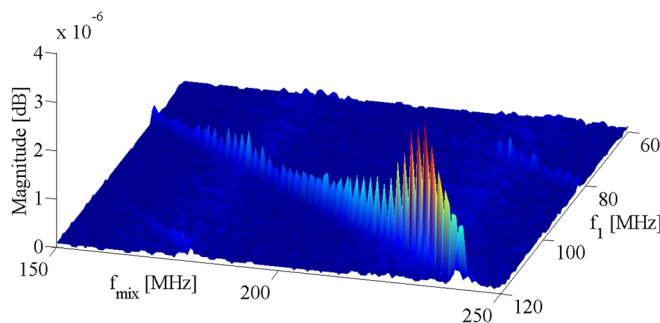

FIG. 6. Magnitude of v_{mix} signal ($P_{in} = -12$ dBm and gate voltage $U_g = +10$ V).
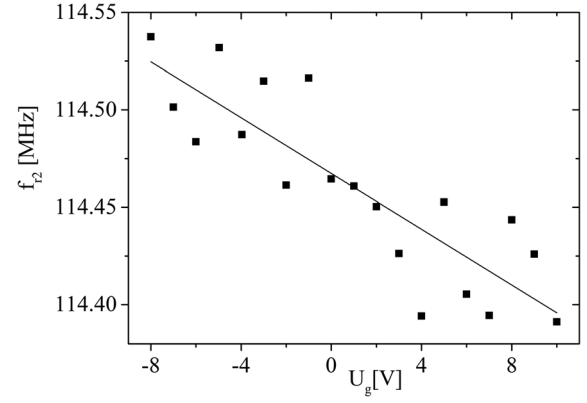

FIG. 7. The resonance frequency f_{r2} dependence on the gate voltage measured with the setup presented in Fig. 5 (the solid line is a guide to an eye).

on U_g suggested weak effect of the gate voltage on the conductivity and on the tension. Therefore, one could assume that particles adsorbed on the surface of the graphene sheet could increase its resonance frequency. However, this does not explain the decrease of the full width at half maximum (FWHM) of the resonance in the second experiment with respect to the FWHM obtained in the first experiment (Fig. 8).

Second factor affecting the resonance of the graphene MEMS is the power actuating its vibrations. To observe the resonance with the second setup (Fig. 5), the power of -12 dBm was applied to the MEMS (which was bigger when comparing to the power applied in the first experiment (Fig. 2)).

Large value of the driving power leads to nonlinear oscillation of the graphene sheet.[28,29] Because of the increasing driving force, the amplitude of the MEMS oscillations increases making the resonator stiffer, which results in a higher resonance frequency. The frequency shift is nonlinear function of the actuating voltage.[11,28] Moreover, due to the damping effect the FWHM of the resonance, which is related to the quality factor Q, decreases.[28]

In the case of our graphene MEMS, both factors should be taken into account to explain the difference between the value of the resonance frequency obtained in the two experiments ($f_{r1} = 103.56$ MHz and $f_{r2} = 114.45$ MHz at $U_g = 0$ V).
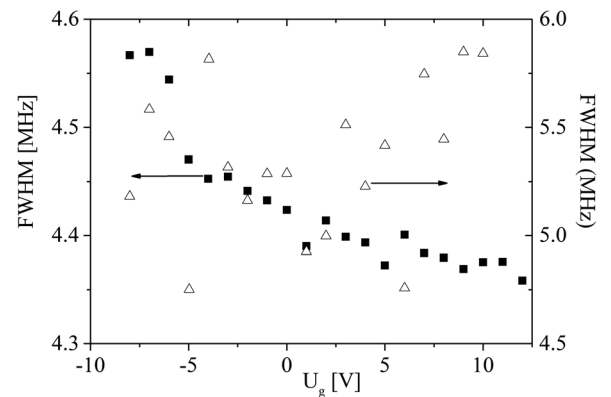

FIG. 8. FWHM of the resonance peak determined from the first experiment (full squares) and from the second experiment (empty triangles) for several gate voltages.

The difference in values of FWHM of the resonance in both experiments (Fig. 8) may result not only from the large driving power but also from the resolution of the oscilloscope. The limit of 500 data points collected by the FFT module during one acquisition process affects the quality of the peak observed on the screen. As a consequence of the above-mentioned limit of 500 data points, the determination of the resonance frequency (Fig. 7) is less accurate when compared to that obtained from the first experiment (Fig. 3).

The resonator's quality depends on the dR/dU_g value. The higher it is, the more sensitive to the change in the gate voltage is the resonator. Our graphene-based resonator shows $dR/dU_g = 107.5$ [Ω/V]. Close to the Dirac point of the graphene sheet one can expect at least one order of magnitude higher value of the dR/dU_g and consequently a pronounced resonance can be observed. Despite the low quality factor of the resonator, the resolution of the setup is good enough to detect its vibrations. Taking into account parameters of the new setup, especially of the oscilloscope, one can state that the new setup can be widely applied, however, to a certain limit.

V. CONCLUSIONS

The experimental setup consisting of the oscilloscope equipped with the FFT was designed and successfully tested. In contrast to that described in the introduction experiments based on mixing technique, our experimental setup was based on the analysis of the signal reflected from the vibrating resonator. The reflected signal was decoupled from the signal driving the vibration. The clear signal related with the resonance was amplified and analyzed by the oscilloscope. Replacement of the VNA with the oscilloscope made the setup portable, allowing a fast tracing of the resonance and analysis of its frequency. The final result of the measurement, i.e., determination of the resonance frequency, depends not only on the resolution of setup but also on the quality of the resonator. Improvement of the graphene quality will result in better quality of the signal analyzed by the oscilloscope and consequently in higher accuracy in determination of the resonance frequency of the graphene MEMS.

[1]S. Tadigadapa and K. Mateti, Meas. Sci. Technol. **20**, 092001 (2009).
[2]S. Basu and P. Bhattacharyya, Sens. Actuators, B **173**, 1 (2012).
[3]S. Xia, T. Shi, D. Liu, L. Xu, H. Long, W. Lai, and Z. Tang, Sens. Actuators, A **198**, 15 (2013).
[4]A. Uranga, J. Verd, E. Marigó et al., Sens. Actuators, A **197**, 88 (2013).
[5]H. B. Nguyen, V. Ch. Nguyen, V. T. Nguyen, H. D. Le, V. Q. Nguyen, T. T. T. Ngo, Q. P. Do, X. N. Nguyen, N. M. Phan, and D. L. Tram, Adv. Nat. Sci.: Nanosci. Nanotechnol. **4**, 015013 (2013).
[6]S. Nomura, Y. Hanasaka, H. Ogawa, M. Hasegawa-Ohira, and T. Ishiguro, *Proceedings of the IEEE International Conference on Systems, Man and Cybernetics*, Anchorage, Alaska, USA, October 9–12, 2011.
[7]A. M. Popov, Y. E. Lozovik, S. Fiorito, and L'H. Yahia, Int. J. Nanomedicine **2**(3), 361–372 (2007).
[8]Ch. Lee, C. Wei, X. D. Kysar, and J. W. Hone, Science **321**, 385 (2008).
[9]K. Bolotin, K. Sikes, Z. Jiang, M. Klima et al., Solid State Commun. **146**, 351 (2008).
[10]Y. T. Yang et al., Nano Lett. **6**, 583 (2006).
[11]Ch. Chen, S. Rosenblatt, K. I. Bolotin et al., Nat. Nanotechnol. **4**, 861 (2009).
[12]Y. Xu, C. Chen, V. V. Deshpande, F. A. DiRenno, A. Gondarenko, D. B. Heinz, S. Liu, P. Kim, and J. Hone, Appl. Phys. Lett. **97**, 243111 (2010).
[13]X. Song, M. Oksanen, M. A. Sillanpää et al., Nano Lett. **12**, 198 (2012).
[14]A. M. van der Zande, R. A. Barton et al., Nano Lett. **10**, 4869 (2010).
[15]F. Schedin A. Geim, S. V. Morozov et al., Nature Mater. **6**, 652 (2007).
[16]S. Rumyantsev, G. Liu, M. S. Shur, R. A. Potyrailo, and A. A. Balandin, Nano Lett. **12**, 2294 (2012).
[17]R. Pearce, T. Iakimov et al., Sens. Actuators, B **155**, 451 (2011).
[18]S. S. Verbridge, H. G. Craighead, and J. M. Parpia, Appl. Phys. Lett. **92**, 013112 (2008).
[19]A. Isacsson, Phys. Rev. B **84**, 125452 (2011).
[20]J. Atalaya, J. M. Kinaret, and A. Isacsson, EPL **91**, 48001 (2010).
[21]Y. Ren, C. Zhu, W. Cai, H. Li, H. Ji et al., Appl. Phys. Lett. **100**, 163114 (2012).
[22]V. Gouttenoire, T. Barois, S. Perisanu, J.-L. Leclercq, S. Purcell, P. Vincent, and A. Ayari, Small **6**(9), 1060 (2010).
[23]V. Sazonova, Y. Yaish et al., Nature **431**, 284 (2004).
[24]J. S. Bunch, A. M. van der Zande, S. S. Verbridge, I. W. Frank et al., Science **315**(5811), 490 (2007).
[25]C. Chen and J. Hone, Proc. IEEE **101**, 1766 (2013).
[26]J. Lee and P. X.-L. Feng, *2012 IEEE International Frequency Control Symposium (FCS),* Baltimore, MD, 21–24 May 2012 (IEEE, 2012), pp. 1–7.
[27]V. Singh et al., Nanotechnology **21**, 165204 (2010).
[28]A. Eichler, J. Moser, J. Chaste, M. Zdrojek, I. Wilson-Rae, and A. Bachtold, Nat. Nanotechnol. **6**, 339 (2011).
[29]S. H. Lee, B. Min, S. S. Lee, S. Il Park, and K.-Ch. Lee, Appl. Phys. Lett. **97**, 183108 (2010).